Recent Progress in Sciences

Science Publication Inc.

Research article Open Access

Energy and water balance assessments in a rainfed corn crop by using aerial camera onboard unmanned aerial vehicle

Antônio Teixeira [1, *], Diego Loureiro [2], Richard Souza [2], Jlyel Cruz [2], Maria Gonzaga [2], Janice Leivas [3], Celina Takemura [3], André Almeida [2]

[1] Corresponding author: Federal University of Sergipe (UFS), São Cristóvão-SE, Brazil

[2] Federal University of Sergipe (UFS), São Cristóvão-SE, Brazil

[3] Embrapa Territory, Campinas-SP, Brazil

[*] Correspondence: Antônio Teixeira. email: heribertoteixeira11@gmail.com; heriberto@academico.ufs.br

Received: September 09, 2025; Revised: December 05, 2025; Accepted: February 14, 2026; Published: February 28, 2025

Abstract

Energy and water balance assessments were caried out an unmanned aerial vehicle (UAV) in rainfed corn crop. The effects of nitrogen (N) fertilizing cover levels were analyzed for supporting precision agriculture. Strong differences in the magnitude of the energy and water balance components were perceived according to the levels of N cover fertilizations along the crop stages, but the ratios of latent (λE) and sensible (H) heat fluxes to net radiation (R_n) stabilizing with N at 200 kg ha^{-1}. The average R_n values ranged from 4.2 MJ m^{-2} d^{-1} to 9.8 MJ m^{-2} d^{-1}; for λE, the rates were from 2.0 MJ m^{-2} d^{-1} to 8.0 MJ m^{-2} d^{-1}; for H from -1.2 MJ m^{-2} d^{-1} to 3.6 MJ m^{-2} d^{-1}; and for G between 0.1 MJ m^{-2} d^{-1} and 0.7 MJ m^{-2} d^{-1}. These values returned to different energy partitions, averaging 43 to 113% for $\lambda E/R_n$, -17% to 54% for H/R_n, and 2% to 7% for G/R_n. The evapotranspiration fraction (E_f), i.e., the ratio of λE to available energy (R_n – G) and r_s were taken as root-zone moisture indicators, both presenting high correlations with field measured biomass production (BIO), and productivity (Pr), with R^2 above 0.90. Comparing Pr with E_f, the highest correlation when plants were with six leaves indicated that corn yield can be estimated from the modelled root zone moisture before harvest. The most important finding is that the models can be applied to estimate λE and H with high resolution aerial cameras without the thermal bands. The energy and water balance modelling demonstrated suitability for corn crop management, indicating the potential for applying these equations in other climatically suitable regions.

Keywords Net radiation, latent heat flux, sensible heat flux, remote sensing

1. Introduction

Nitrogen (N) cover applications in corn crops is an important practice to promote high biomass production (BIO) and productivity (Pr), but care needs to be taken to minimize environmental impacts by N lixiviation to ground water. These impacts highlight energy and water balance assessments under different crop fertilization managements to minimize impacts while maintaining good productivity levels, mainly in scenarios of climate and land use changes [1, 2]. Under good root-zone moisture conditions, the highest portion of the available energy is for the latent heat flux (λE), favoring BIO and Pr [3], while during dry periods, the large amount of net radiation (R_n) is partitioned as sensible heat fluxes (H), promoting heating [4]. Accounting the fraction $\lambda E/R_n$ in agricultural crops is highlighted as this ratio represents the fraction of the available energy used for evapotranspiration [5, 6], which is partitioned into transpiration and soil evaporation, depending on the atmospheric demand, root-zone moisture and crop stages [7].

Although high $\lambda E/R_n$ favoring yield, intensive agricultural growing regions can mean reductions of water availability to other sectors, while the H/R_n values can indicate warming or cooling conditions [4, 8]. Increases on H and reductions on λE, have been reported because replacement of Atlantic Forest species by sugarcane crop, in Southeast Brazil and when this replacement happened with coffee the opposite situation was verified [6]. At daily scales, the portion of R_n partitioned into soil heat flux (G) is small and it is generally neglected in energy and water balance studies [8, 9]. Assessing the energy and water balance components describing their dynamics in rainfed and irrigated crops under different managements at good spatial

resolutions is meaningful to support sustainable agricultural expansions [3]. Besides fertilization management in corn crops, agrometeorological conditions drive these balances under both irrigated [10] and rainfed [1] conditions. Water deficit during dry seasons is the most important weather factor which reduces BIO and Pr [11]. To attain high Pr levels, good crop management is required, which in turn affects the energy partitions into λE and H [1].

Field measurements on energy and water balances at high spatial scales are time and cost intensive, highlighting the use of geotechnologies for this task [1, 2, 10]. Remote sensing together with agrometeorological data is a strong tool to monitor energy [5, 6] and water [12] balance components along the corn crop stages, when aiming at high BIO and Pr, while minimizing negative environmental impacts [1, 3]. These components vary, spatially and temporally, along the crop stages according to vegetation and moisture conditions which in turn are influenced by nitrogen (N) cover fertilization levels in corn crops [1, 13]. Quantifying the energy and water balance partitions is important to assist farmers with in-depth crop monitoring and high spatial resolution remote sensing data from aerial cameras onboard unmanned aerial vehicles (UAV) can be accurately used for these assessments [1, 14-16]. The acquired data offer spectral, spatial, and temporal resolution, providing detailed vegetation and nutrient status; growth vigor, and can be used for yield prediction, being possible combinations of UAV products with other spatially information [14]. UAV measurements have potential to improve environmental monitoring, offering opportunities to bridge the gap between field observations and satellite remote sensing, by providing high spatial detail in a cost-effective way and capacity for enhanced temporal resolution [15]. Significant correlations between NDVI and leaf area index values from a UAV platform and spectroradiometer were reported over sunflower crop [16].

High resolution remote sensed images from UAV can guide rational N cover fertilizations in agricultural crops [17], but this is a challenging task, and besides spectral responses through UAV, other methods are in use, including handheld sensors, and satellite imagery. The use of UAV and satellite imagery for this task is better compared to conventional methods such as soil testing [18]. Even with the advances of aerial cameras overcoming cloudy problems from satellite images their use demands tests with field data for practical applications [19]. According to [17], crop sensing technologies to N cover fertilization management in grain crops have been the focus of an important element of Precision/Digital Agriculture research and field measurements adopted in most studies are not the ideal method to evaluate the effects of spatial variability, confirming that new approaches are needed based on the use of multiple sensors. Reflectance indices are useful to detect water stress in distinct crops, and UAVs give opportunities to monitor crop fields with high spatial and temporal resolution images comparing with ground-truth plant data [19].

The energy partition into λE affects plant development and physiological processes impacting BIO and Pr in corn crops [20, 21]. These crop yield parameters are highly variable in both space and time in agriculture, and these variations can be detected by remote sensing reflectance pixel values [22]. Many ways arise for raising BIO and Pr in agriculture under rainfed and irrigation conditions [23]. For rainfed crops, the main challenge is to do this through optimized management practices [24]. Spatially determining the factors which affect BIO is strongly useful to analyze the feasibility of setting up new biomass power plants, such as corn crops, to optimize the best locations for agricultural expansion [25], and to support public policies regarding rational environmental managements to improve Pr [26]. One of the main ways for optimizing BIO and Pr in corn crops is through crop and water management which include N cover fertilization improvements [1, 17].

Distinct remote-sensing algorithms have been used for energy, water and carbon balance assessments in agriculture. Due to its operationality while maintaining its physical basis, some of them use the Penman–Monteith equation for these assessments [3, 10, 12, 27]. In the current study, to retrieve the energy and water balance components and related them to measured corn BIO and Pr, the SUREAL (Surface Resistance Algorithm), based on the Peman Monteith equation, was applied with a Mapir camera onboard an UAV to estimate the r_s, retrieving λE. The algorithm was developed by using simultaneous field and remote sensing measurements in Northeast Brazil. The bands 1 to 7 from Landsat 5 satellite were used together with micrometeorological data to derive and validate all the SUREAL's equations [28, 29]. After elaboration, it has been validated under distinct agroecosystems by using different remote sensing platforms in Northeast Brazil [3]. The reason for SUREAL's choice, besides its applicability, another important advantage, regarding other algorithms, is that there is no need for thermal bands, it being possible to use only the reflectance bands of an aerial camera onboard a UAV.

In Northeast Brazil, the use of UAV technologies for rainfed corn crop management is suitable because high probabilities of frequent dry weather events affecting BIO and Pr. These crop yield parameters are closed related to the energy, carbon and mass transfer between vegetation and the lower atmosphere and there are still few studies with high-resolution images for modelling these transferences and their relations in rainfed corn crop within the Brazilian Atlantic Forest biome. Few ones were carried out with specific cultivars and environments using Landsat 8 images for corn under irrigation conditions [12, 30], for rainfed corn crop with UAV in the Caatinga biome [1]; and for irrigated corn crop with UAV in the Savana biome [10]. In the Atlantic Forest biome inside Northeast Brazil, the ecosystems are experiencing environmental impacts by climate

and land use changes which affect the available energy partitions into λE and H. These changes can increase water consumption or warm conditions. This is the actual scenario in agricultural growing areas, where corn has been cultivated for grain consumption and for silo, but also as a biofuel option.

The energy and water balance assessments were carried out during eight rainfed corn crop stages and for its growing season with distinct nitrogen (N) cover fertilization levels; considering the effects on crop yield and environmental problems which could happen by leaching this nutrient to the groundwater [1]. With field measurements of BIO and Pr, besides assessing the dynamics of the remote sensing energy and water balance components for different N cover fertilization levels with urea N source, their relationships with these crop parameters were also analyzed. For this task it was used the reflectance bands of aerial images of a Mapir camera onboard an UAV, in a rainfed corn crop within the Atlantic Forest biome within Northeast Brazil. Besides monitoring these components along the crop stages, the results are useful for recommendation of rational fertilization levels and water requirements when aiming to improve corn yield minimizing negative environmental impacts.

The authors expect that, with the success of these specific applications for the corn reference crop within the Brazilian Atlantic Forest biome, the models could be used in other regions and crops probably only requiring corrections for the calibration coefficients of the modelling equations to infer distinct environmental and management conditions. Our hypothesis is that energy and water balance components can be assessed with the reflective bands of a sensor onboard an UAV together with weather data and these assessments can be useful to quantify the effect of crop fertilization managements allowing to predict BIO and Pr before the harvest time, supporting farmers for rational decisions about post-harvest actions.

2. Material and methods

For this research we used remote sensing images collected from an aerial camera onboard an UAV together with weather data and field measurements of crop parameters described as following.

2.1 Experimental field and N cover fertilization levels

Figure 1 presents location details of the corn crop area and N cover fertilization levels.

The study was in the São Cristóvão County, Northeast Brazil, latitude 11°01′ S, longitude 37°00′ W, and altitude of 30 m, a region of tropical sub-humid climate within the Atlantic Forest biome [31]. The region presents a mean air temperature (T_a) of 25.2°C, annual precipitation (P) of 1331 mm, concentrated from March to August. The soil is classified as Red Yellow Argisol, with wavy relief and natural ecosystems are forests which are being replaced by agricultural crops [32]. Cover fertilizations were with urea N source (46% of N) at different N levels (L), with N levels at 0 kg ha^{-1} (L0), 25 kg ha^{-1} (L1), 50 kg ha^{-1} (L2), 100 kg ha^{-1} (L3), 200 kg ha^{-1} (L4), and 400 kg ha^{-1} (L5). Following [33] the crop stages adapted for the studied SHS 7939 PRO2 cultivar involved: sowing (S); emergency (E); vegetative stages with four, six, and ten leaves (V4, V6, and V10); pre-flowering (PF); full flowering (FF); grain filling (GF); physiological maturation (PM); and harvest (Hvt). The UAV flights were carried out from E to PM.

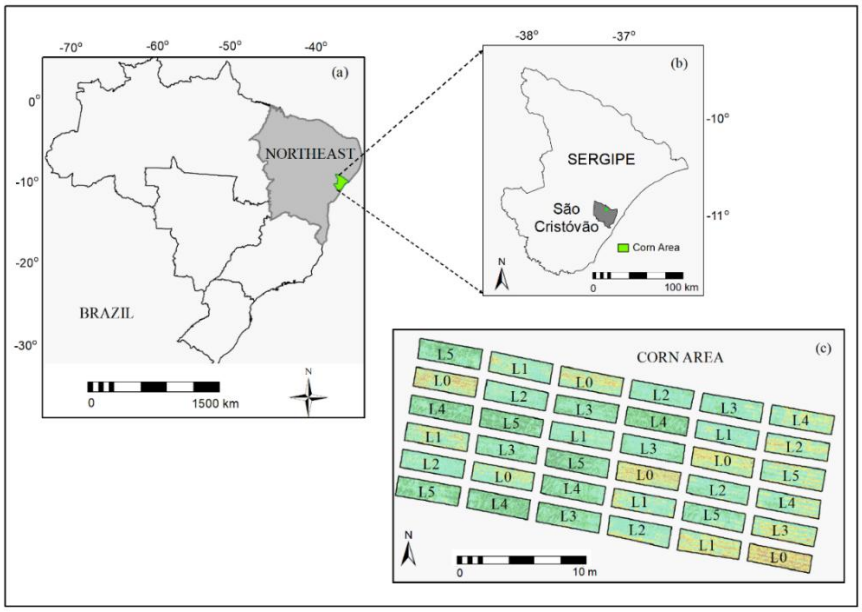

Figure 1 Location of the corn crop area. (a) Sergipe state in Northeast Brazil; (b) São Cristóvão County, and (c) Nitrogen (N) cover fertilization levels (L).

2.2 Data acquisitions and processing

The UAV flights were around noon time at 60 m height, resulting in a spatial resolution of 0.05 m, during the crop stages E (July 17); V4 (July 28); V6 (August 04); V10 (August 18); PF (September 01); FF (September 13); GF (September 22); and PM (October 06) in the year 2022. To construct the mosaics the software "Agisoft Photoscan 1.3.5" was used resulting in longitudinal and lateral overlaps of 80% and 75%, respectively. From digital numbers (DN) of bands 1 to 3 of the Mapir Camera, the reflectance (ρ) values were retrieved with a calibration panel [34]. Daily weather data from one station close to the experimental were used together with remote sensing parameters for the modelling steps [3, 9, 28].

To relate the energy and water balance components with crop parameters, BIO and Pr were measured at the end of the corn growing season for each N cover fertilization level. After PM, the vegetative and reproductive parts of corn plants were cut, weighed, and dried, and fresh matter obtained upscaling the dry samples. The ratio of the dry to the fresh matter of the crushed sample was multiplied by the total matter to retrieve BIO, while Pr was obtained after correcting moisture. From these crop measurements, it was also possible to relate remote sensing root-zone moisture indicators to field BIO and Pr values for each N cover fertilization level in the corn growing season.

2.3 Modelling energy and water balance components

Following [9], the latent heat flux - λE (MJ m^{-2} d^{-1}) was retrieved by the Penman-Monteith equation, modelling net radiation (R_n), soil heat flux (G), surface resistance (r_s) and aerodynamic resistance (r_a) from remote sensing measurements, together with weather data [28].

According to [35], we used the Slob equation to estimate the daily R_n values (W m^{-2}):

$$R_n = (1 - \alpha_0)R_G - a_L\tau \quad (1)$$

where α_0 is the surface albedo (-); R_G (W m^{-2}) was measured global solar radiation; τ is the atmospheric transmissivity; and a_L is a regression coefficient [1-3, 8]. For G (MJ m^{-2} d^{-1}) it was assumed its ratio to R_n according to [28] and to acquire α_0, the Planck's law was used, integrating the radiation over the wavelength intervals for each Mapir band considering their fractions over the solar spectrum [1, 5].

$$\alpha_0 = \sum W_{band}\,\rho_{band} \quad (2)$$

where the w_{band} is the weight of 0.42; 0.35; and 0.23 for the bands 1, 2, and 3 of the Mapir camera.

To estimate r_s (s m^{-1}) the SUREAL algorithm was applied:

$$r_s = \exp\left[a_r\left(\frac{T_0}{\alpha_0}\right)(1 - NDVI) + b_r\right] \quad (3)$$

where T_0 (°C) is the surface temperature, NDVI is the Normalized Difference Vegetation Index, and the regressions coefficients a_r and b_r are 0.04 and of 2.72 [3, 28], with NDVI calculated according to [36] as the ratio of the difference of the reflectance values in the near infrared and red bands by their sum

Without a thermal band in the Mapir camera, T_0 (K) was retrieved by the residual method applying the Stefan-Boltzmann equation to estimate the long-wave radiation components [37]:

$$T_0 = \sqrt[4]{\frac{R_G(1 - \alpha_0) + \sigma\varepsilon_a {T_a}^4 - R_n}{\sigma\varepsilon_0}} \quad (4)$$

where T_a is the measured air temperature in K; ε_a is the atmospheric emissivity calculated as a function of τ, R_n (W m^{-2}) is the net radiation, σ is the Stefan-Boltzmann constant (5.67 × 10^{-8} W m^{-2} K^{-4}), and ε_0 is the surface emissivity estimated from NDVI [3, 8, 28].

According to [9] the transfer of heat and water vapor from the evaporating surface into the air above the canopy is determined by the aerodynamic resistance (r_a):

$$r_a = \frac{\ln\left(\frac{z_2 - d}{z_{0m}}\right)\ln\left(\frac{z_2 - d}{z_{0h}}\right)}{k^2 u_2} \quad (5)$$

where z_2 is the height of wind speed and humidity at 2m; z_{0m} is roughness length governing momentum transfer (m); d is the zero plane displacement height (m) assumed as $4.67z_{0m}$; z_{0h} (m) is the roughness length governing of heat and vapor transfer (m), considered as $0.135z_{0m}$; k of 0.41 (-) is the von Karman's constant; and u_2 is the wind speed at z_2 (m s^{-1}); being z_{0m} estimated by:

$$z_{0m} = \exp\left[\left(a_z\frac{NDVI}{\alpha_0}\right) + b_z\right] \quad (6)$$

where a_z and b_z are regression coefficients of 0.24 and -2.12, respectively [28].

Having R_n, λE, and G estimated, H was acquired by residue in the energy balance equation and E_f considered as the ratio of λE to the available energy (R_n – G) [5, 8].

2.4 Statistical analysis

For statistical analyzes, besides analyzing averages and standard deviations (SD) of the energy and water balance components for all experimental area and for each corn parcel, we used the 2-way ANOVA (Analysis of Variance) in R to carry out a pairwise comparison through the Tuckey honestly significant difference (HSD) post-hoc test, regarding R_G used as R_n and energy partitions into λE, H and G, at 5% significance level, considering the six N cover fertilizing levels (L0 = 0 kg ha^{-1}, L1 = 25 kg ha^{-1}, L2 = 50 kg ha^{-1}, L3 = 100 kg ha^{-1}, L4 = 200 kg ha^{-1}, and L5 = 400 kg ha^{-1}), and the UAV flights at eight CS: E, V4, V6, V10, PF, FF, GF, and PM [1].

3. Results and discussion

After processing the remote sensing and field data, the results are discussed in terms of the dynamics of the

energy and water balance components for each CS and N cover fertilization levels as well as their correlations with measured crop parameters for the corn crop growing season.

3.1 Environmental conditions

The average daily values for R_G and T_a, together with the corresponding totals for precipitation (P) and reference evapotranspiration (ET_0) during the corn growing season are shown in Figure 2, in terms of Day of the Year (DOY).

According to Figure 2a, the largest R_G, with average higher than 20.0 MJ m^{-2}, and T_a, above 26.0°C, were from DOY 258 (September) to DOY 321 (November); while the lowest corresponding values were between DOY 187 (July) and DOY 235 (August), when dropped to below 15.0 MJ m^{-2} d^{-1} and 20.0°C, respectively. From Figure 2b, rainfall was concentrated between DOY 186 (July) and DOY 246 (September), when P surpassed 20 mm d^{-1} and the highest ET_0 happened from DOY 275 (October) to DOY 321 (November), above 5.5 mm d^{-1}. Considering the P of 351.4 mm and ET_0 of 551.6 mm for the corn growing season, respectively, rainfall accounted for 64% of ET_0. These weather dynamics showed that the best corn root-zone moisture conditions happened from July to September, but under the lowest atmospheric demands, which limited λE somewhat, even under good rainfall-water availability.

3.2 Energy balance components

Having acquired the corn energy balance components pixel by pixel, their spatial and temporal variations were statistically analyzed, as well as their correlations with field measured crop yield parameters.

3.2.1 Spatial and Temporal Variations in Net Radiation (R_n)

Figure 3 presents the R_n spatial distributions together with its pixel averages and SD, regarding the whole corn area (a) and for each N cover fertilization level – L (b), considering the analyzed corn crop stages.

From Figure 3a, there was a clear increase on R_n values along the crop stages, with average values for the whole corn area between 4.0 and 7.0 MJ m^{-2} d^{-1} from E (July 17) to V6 (August 04), reaching a mean of 9.8 MJ m^{-2} d^{-1} in GF (September 22). Spatial variations also raised along the crop stages, with SD representing 7% of the average from E to V6 (July 17 – August 04) to 19% of the mean pixel value in PM (October 06). However, according to Figure 3b, although R_n values change along the crop stages, an average pixel value of 7.4 MJ m^{-2} d^{-1} for the corn growing season is found for any specific N cover fertilization level (L0 to L5), evidencing that the most change in R_n values are due variations on R_G levels.

Table 1 shows the R_n/R_G average and SD values from remote sensing measurements and weather data, together with the results of the pairwise comparison by group, using the Tuckey HSD post-hoc test performed for the N cover fertilization levels for each corn CS.

Crossing the R_n and R_G values it is possible to see that even having variations on R_n/R_G values along the growing season, there were no significative differences from the Tuckey HSD post-hoc test among N cover fertilization levels within a specific CS. Averages ranged from a minimum of 0.37 in V4 (July 28, DOY 209) for L0 and L1 increasing to peak of 0.48 to 0.50 in PF (September 01, DOY 244), with SD representing in average 7% of the average pixel value from E to V4 to 21% in PM. Overall R_n/R_G average of 0.43 means that in general 43% of R_G was partitioned into λE, H and G considering all N cover fertilizations levels and crop stages.

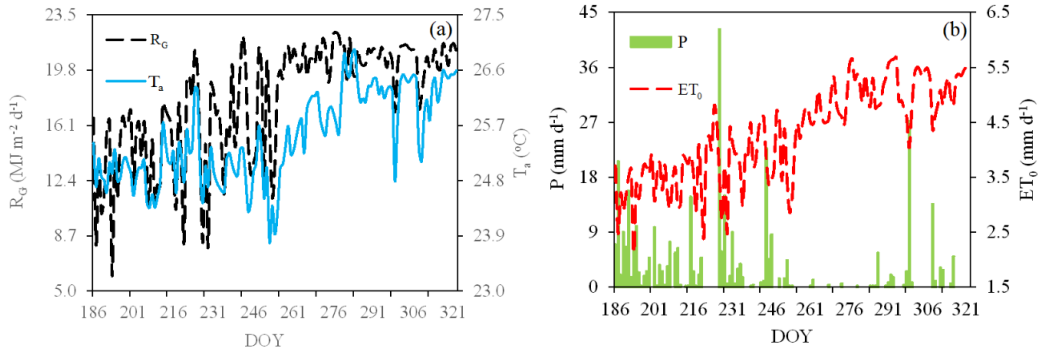

Figure 2 Weather data during the corn growing season in 2022 in terms of the Day of the Year (DOY). (a) Daily mean values for global solar radiation (R_G) and mean air temperature (T_a); and (b) Daily totals for precipitation (P) and reference evapotranspiration (ET_0).

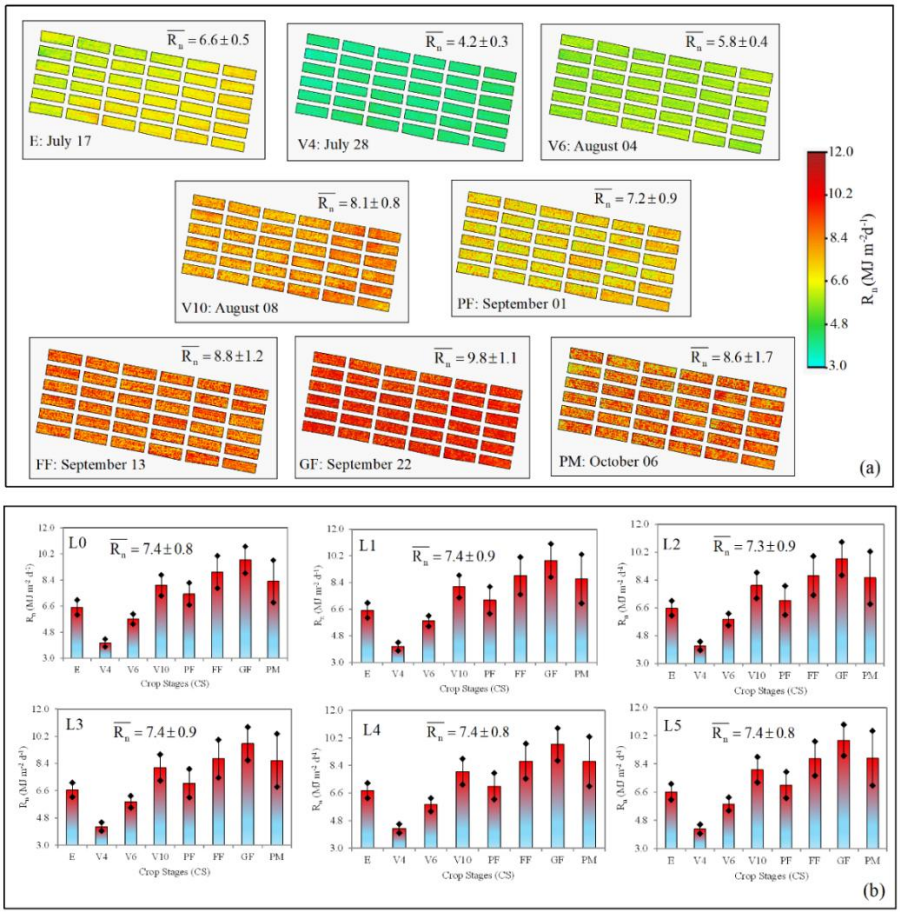

Figure 3 Spatial distribution of daily net radiation (R_n), together with its averages and standard deviations (SD), regarding the whole experimental area (a) and for each N cover fertilization level – L[1] (b), involving the analyzed corn crop stages – CS[2], during the year 2022. [1]L: L0 – N at 0 kg ha^{-1}; L1 – N at 25 kg ha^{-1}; L2 – N at 50 kg ha^{-1}; L3 – N at 100 kg ha^{-1}; L4 – N at 200 kg ha^{-1}; and L5 – N at 400 kg ha^{-1}. [2]CS: E – Emergency; V4, V6, and V10 – Vegetative stages with four, six, and ten leaves, respectively; PF – Pre-flowering; FF – Full flowering; GF – Grain filling; and PM – Physiological maturation.

Table 1 Average pixel values and standard deviations (SD) for the ratio of net radiation (R_n) to incident solar global radiation (R_G) together with the Tuckey HSD post-hoc test performed by group, considering the N cover fertilizing levels for each corn crop stage (CS).

		Ratio of net radiation (R_n) to incident global solar radiation (R_G)						
N levels	CS[2]	L0: 0 (kg ha^{-1})	L1: 25 (kg ha^{-1})	L2: 50 (kg ha^{-1})	L3: 100 (kg ha^{-1})	L4: 200 (kg ha^{-1})	L5: 400 (kg ha^{-1})	Average
[1]DOY								
198	E	0.41 ± 0.03a	0.41 ± 0.03a	0.41 ± 0.03a	0.42 ± 0.03a	0.42 ± 0.03a	0.41 ± 0.03a	0.41 ± 0.03
209	V4	0.37 ± 0.02a	0.37 ± 0.03a	0.38 ± 0.02a	0.38 ± 0.03a	0.39 ± 0.03a	0.39 ± 0.03a	0.38 ± 0.03
216	V6	0.44 ± 0.05a	0.44 ± 0.05a	0.45 ± 0.05a	0.45 ± 0.05a	0.45 ± 0.05a	0.45 ± 0.05a	0.45 ± 0.05
230	V10	0.42 ± 0.05a	0.43 ± 0.05a	0.43 ± 0.05a	0.43 ± 0.05a	0.42 ± 0.05a	0.42 ± 0.05a	0.43 ± 0.05
244	PF	0.50 ± 0.06a	0.48 ± 0.07a	0.48 ± 0.07a	0.48 ± 0.07a	0.47 ± 0.07a	0.47 ± 0.07a	0.48 ± 0.07
256	FF	0.45 ± 0.06a	0.45 ± 0.07a	0.44 ± 0.07a	0.44 ± 0.07a	0.44 ± 0.06a	0.44 ± 0.06a	0.44 ± 0.07
265	GF	0.45 ± 0.05a	0.46 ± 0.06a	0.45 ± 0.06a	0.45 ± 0.06a	0.45 ± 0.06a	0.46 ± 0.06a	0.45 ± 0.06
279	PM	0.39 ± 0.07a	0.41 ± 0.08a	0.40 ± 0.08a	0.41 ± 0.09a	0.41 ± 0.08a	0.41 ± 0.09a	0.41 ± 0.09
Average	-	0.43 ± 0.05	0.43 ± 0.06	0.43 ± 0.05	0.43 ± 0.06	0.43 ± 0.05	0.43 ± 0.06	0.43 ± 0.05

[1]DOY – Day of the Year

[2]CS: Crop stages; E – Emergence; Vegetative stages: V4 – Plants with four leaves per plant; V6 – Plants with six leaves per plant, and V10 – Plants with ten leaves per plant; Reproductive stages: PF – Pre flowering, FF – Full flowering, GF - Grain filling, and PM- Physiological maturation.

The R_n/R_G values with the same letter in each line indicate no significant differences from each other at 5% (pairwise comparisons using the Tuckey HSD post-hoc test performed by group with six repetitions for each CS.

R_n/R_G values ranging from 41% to 47% with Landsat images were reported in Northeast Brazil independently of the agroecosystem type [5]. However, these assessments included well irrigated fruit crops, besides natural vegetation of the Brazilian Caatinga biome, under different rainfall and irrigation water availability. By field energy balance experiments in a path of the Brazilian Atlantic Forest biome, R_n was around 40 to 68% of R_G [38]. This higher range is that the study area in São Paulo city involved mixed conditions of autumn-winter and spring-summer within the metropolitan area, contrasting with our current results during the rainy growing season of corn crop in Northeast Brazil.

3.2.2 Spatial and Temporal Variations in Latent Heat Flux (λE)

Figure 4 presents the λE spatial distributions together with its pixel averages and SD, regarding the whole corn area (a) and for each N cover fertilization level – L (b), considering the analyzed corn crop stages.

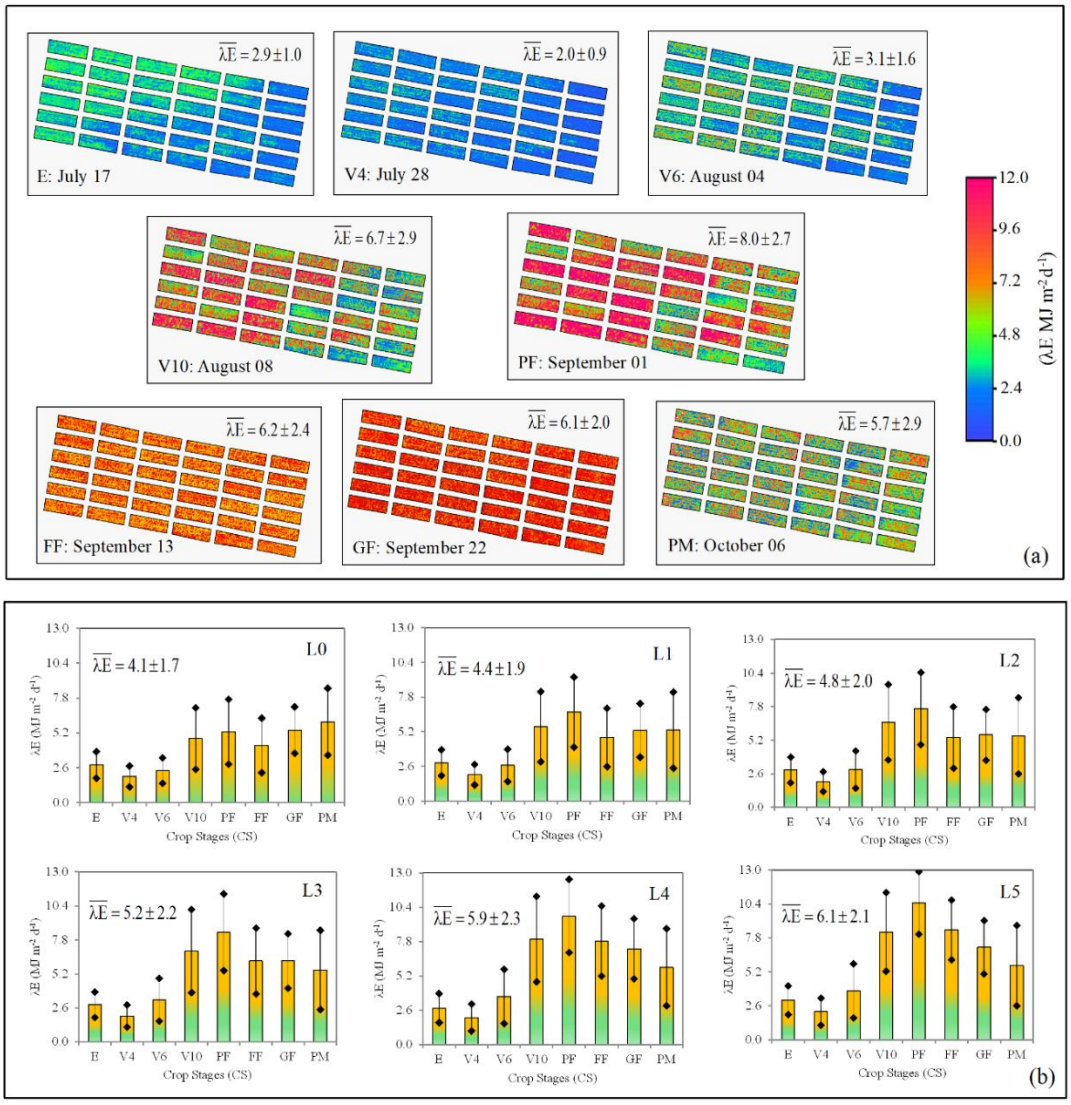

Figure 4 Spatial distribution of daily latent heat fluxes (λE), together with its averages and standard deviations (SD), regarding the whole experimental area (a) and for each N cover fertilization level – L[1] (b), involving the analyzed corn crop stages – CS, during the year 2022. [1]L: L0 – N at 0 kg ha^{-1}; L1 – N at 25 kg ha^{-1}; L2 – N at 50 kg ha^{-1}; L3 – N at 100 kg ha^{-1}; L4 – N at 200 kg ha^{-1}; and L5 – N at 400 kg ha^{-1}. [2]CS: E – Emergency; V4, V6, and V10 – Vegetative stages with four, six, and ten leaves, respectively; PF – Pre-flowering; FF – Full flowering; GF – Grain filling; and PM – Physiological maturation.

Visible λE spatial and temporal are noticed along the crop stages when considered the whole corn crop area (Figure 4a), with averages ranging from 2.0 and 3.1 MJ m^{-2} d^{-1} between July 17 (E) and August 04 (V6), increasing to 8.0 MJ m^{-2} d^{-1} in September 01 (PF), dropping to 5.7 MJ m^{-2} d^{-1} in October 06 (PM). The spatial variations were also large, with SD accounting for 50% of the average in August 04 (V6) to 33% on September 22 (GF). According to Figure 4b, unlike R_n, λE variations are noticed among N cover fertilization levels averaging for the growing season, with the highest ones in PF for L5 in September 01 (mean of 10.5 MJ m^{-2} d^{-1}) while the minimums were for L0 (mean of 2.0 MJ m^{-2} d^{-1}) in V4 (July 28). Besides crop stages and N cover

fertilization levels, the λE rates were also influenced by weather conditions, mainly R_G and P.

In Colorado (USA), λE rates between 4.9 to 6.9 MJ m^{-2} d^{-1} and 7.6 to 9.3 MJ m^{-2} d^{-1} were reported under limited irrigation, with water stressed plants as an effort to maximize water productivity [39]. These ranges involve our average rate of 5.1 MJ m^{-2} d^{-1} under rainfed conditions with some degree of water scarcity in Northeast Brazil. Through field measurements in irrigated corn with mulching in Northwestern China, [40] found higher average daily λE of 8.6 MJ m^{-2} d^{-1}. The authors concluded that the water fluxes were mainly controlled by R_G levels. Their average values under better soil moisture conditions for two growing seasons are like our mean value during the PF stages under high rainfall amounts. From Sequoia camera measurements onboard an UAV over rainfed corn in the drier Brazilian Caatinga biome, [1] reported an average λE of 5.4 MJ m^{-2} d^{-1} under different N cover fertilization levels with urea, close to our average value with the Mapir camera onboard an UAV over corn crop in the Atlantic Forest biome within Northeast Brazil.

The similarities among our results and those from literature under some degree of water stress bring confidence in the suitability for estimating λE by modelling the aerodynamic and surface resistances in the Penman-Monteith equation [3, 28] using the reflectance values of the Mapir camera onboard an UAV together with weather data.

Table 2 shows the $\lambda E/R_n$ average and SD values from remote sensing measurements and weather data, together with the results of the pairwise comparison by group, using the Tuckey HSD post-hoc test performed for the N cover fertilization levels in each corn CS.

Table 2 Average pixel values and standard deviations (SD) for the ratio of latent heat flux (λE) to net radiation (R_n) together with the Tuckey HSD post-hoc test performed by group, considering the N cover fertilizing levels for each corn crop stage (CS).

		Ratio of latent heat flux (λE) to net radiation (R_n)						
N levels	CS[2]	L0: 0 (kg ha^{-1})	L1: 25 (kg ha^{-1})	L2: 50 (kg ha^{-1})	L3: 100 (kg ha^{-1})	L4: 200 (kg ha^{-1})	L5: 400 (kg ha^{-1})	Average
[1]DOY								
198	E	0.43 ± 0.19a	0.44 ± 0.18a	0.44 ± 0.18a	0.43 ± 0.17a	0.41 ± 0.20a	0.46 ± 0.20a	0.43 ± 0.19
209	V4	0.48 ± 0.22a	0.49 ± 0.20a	0.48 ± 0.21a	0.47 ± 0.23a	0.48 ± 0.28a	0.51 ± 0.28a	0.48 ± 0.24
216	V6	0.42 ± 0.18a	0.46 ± 0.23a	0.50 ± 0.28a	0.55 ± 0.32a	0.62 ± 0.40a	0.64 ± 0.41a	0.53 ± 0.30
230	V10	0.59 ± 0.34a	0.69 ± 0.39ab	0.82 ± 0.44ab	0.85 ± 0.47ab	1.00 ± 0.49ab	1.03 ± 0.46b	0.83 ± 0.43
244	PF	0.71 ± 0.40a	0.93 ± 0.46a	1.08 ± 0.48abc	1.18 ± 0.49bc	1.38 ± 0.45bc	1.49 ± 0.40c	1.13 ± 0.45
256	FF	0.48 ± 0.29a	0.54 ± 0.32ab	0.62 ± 0.36ab	0.71 ± 0.37bc	0.90 ± 0.39cd	0.96 ± 0.34d	0.70 ± 0.35
265	GF	0.55 ± 0.23a	0.54 ± 0.27a	0.57 ± 0.27a	0.64 ± 0.29abc	0.74 ± 0.30bc	0.72 ± 0.27c	0.63 ± 0.27
279	PM	0.72 ± 0.40a	0.62 ± 0.42a	0.65 ± 0.42a	0.64 ± 0.43a	0.68 ± 0.43a	0.65 ± 0.43a	0.66 ± 0.42
Average	-	0.55 ± 0.28	0.59 ± 0.31	0.65 ± 0.33	0.68 ± 0.35	0.78 ± 0.37	0.81 ± 0.35	0.67 ± 0.33

[1]DOY – Day of the Year

[2]CS: Crop stages; E – Emergence; Vegetative stages: V4 – Plants with four leaves per plant; V6 – Plants with six leaves per plant, and V10 – Plants with ten leaves per plant; Reproductive stages: PF – Pre flowering, FF – Full flowering, GF - Grain filling, and PM- Physiological maturation.

The $\lambda E/R_n$ values with the same letter in each line indicate no significant differences from each other at 5% (pairwise comparisons using the Tuckey HSD post-hoc test performed by group with six repetitions for each CS.

There were variations on $\lambda E/R_n$ values from E to PM for all N cover fertilization levels (L0 to L5), evidenced by the Tuckey HSD post-hoc test. However, with no significative differences between them from E to V6 and during PM. The daily average $\lambda E/R_n$ ranged from a minimum of 0.42 from E to V6 from DOY 198 (July 17) to 216 (August 04) with L0, increasing to a peak of 1.49 for PF (DOY 244, September 01) with L5. This last average above 1.00 indicates situations of additional energy for water fluxes by heat advection coming from dryer areas to corn parcels [5, 6].

Average $\lambda E/R_n$ values for the corn growing season ranged from 0.55 (L0) to 0.81 (L5), meaning a general good root-zone moisture conditions for BIO and Pr. However, the high SD, representing around 50% of the average pixel values, indicated large spatial variations in soil cover and moisture, which affected energy partitions into transpiration and soil evaporation [41]. These differences were affected by the N cover fertilizations but stabilizing at 200 kg ha^{-1} (L4), meaning that much N is percolated to the ground water above this level without significantly affecting BIO and Pr, what agreed with [1], with N cover applications with urea for rainfed corn crop in the Caatinga Brazilian biome.

3.2.3 Spatial and Temporal Variations in Sensible Heat Flux (H)

Figure 5 presents the H spatial distributions together with its pixel averages and SD, regarding the whole corn area (a) and for each N cover fertilization level – L (b), considering the analyzed corn crop stages.

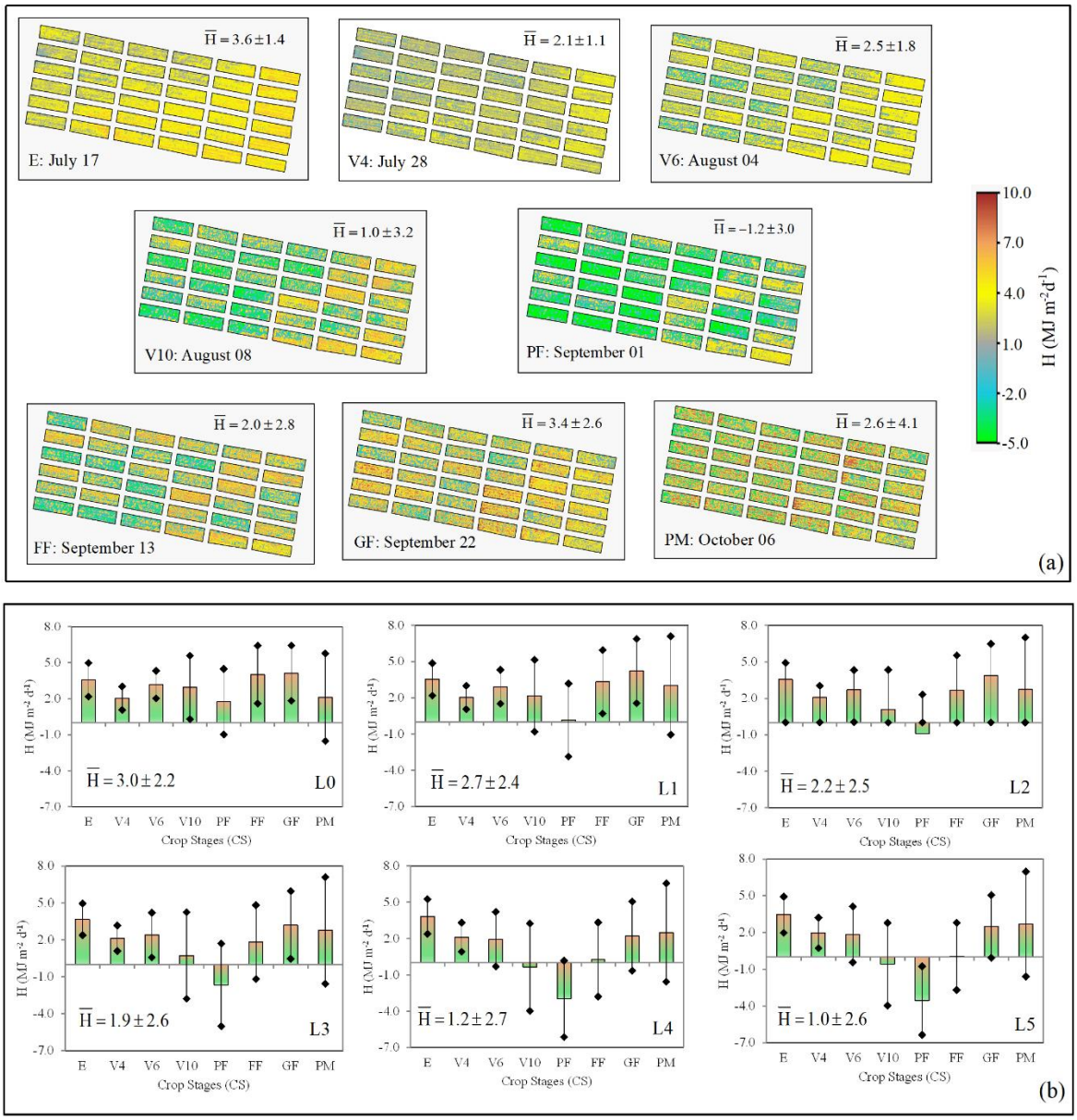

Figure 5 Spatial distribution of daily sensible heat fluxes (H), together with its averages and standard deviations (SD), regarding the whole experimental area (a) and for each N cover fertilization level – L[1] (b), involving the analyzed corn crop stages – CS[2], during the year 2022. [1]L: L0 – N at 0 kg ha^{-1}; L1 – N at 25 kg ha^{-1}; L2 – N at 50 kg ha^{-1}; L3 – N at 100 kg ha^{-1}; L4 – N at 200 kg ha^{-1}; and L5 – N at 400 kg ha^{-1}. [2]CS: E – Emergency; V4, V6, and V10 – Vegetative stages with four, six, and ten leaves, respectively; PF – Pre-flowering; FF – Full flowering; GF – Grain filling; and PM – Physiological maturation.

There was a strong reduction in H rates from E to PF in the whole experimental corn area, reaching a negative average (Figure 5a). The mean pixel values were between 2.1 and 3.6 MJ m^{-2} d^{-1} from July 17 (E) to August 04 (V6), dropping to -1.2 MJ m^{-2} d^{-1} in PF (September 01). From this last CS, the average H increased to above 3.0 MJ m^{-2} d^{-1} from September 22 (GF), declining again in PM (October 06), but with still higher than 2.5 MJ m^{-2} d^{-1} during this last CS. Regarding the spatial variations, the maximum SD occurred during V10, representing more than three times the mean pixel value. The negative average value in PF revealed the highest horizontal heat fluxes from the driest surfaces to corn plants [4-6, 8, 30].

As for λE, also strong variations on H daily values are noticed according to N cover fertilization levels along each CS (Figure 5b), but with the lowest ones during PF for L5 in September 01 (average of -3.6 MJ m^{-2} d^{-1}) and the maximum for L0 (average of 4.2 MJ m^{-2} d^{-1}) in GF (September 22). Besides crop stages, the partition of R_n into H values were also influenced by weather conditions, mainly high R_G levels together with rainfall amounts.

Table 3 shows the H/R_n average and SD values from remote sensing measurements and weather data, together with the results of the pairwise comparison by group, using the Tuckey HSD post-hoc test performed for the N cover fertilization levels in each corn CS.

Table 3 Average pixel values and standard deviations (SD) for the ratio of sensible heat flux (H) to net radiation (R_n) together with the Tuckey HSD post-hoc test performed by group, considering the N cover fertilizing levels for each corn crop stage (CS).

		Ratio of sensible heat flux (H) to net radiation (R_n)						
N levels	CS[2]	L0: 0	L1: 25	L2: 50	L3: 100	L4: 200	L5: 400	Average
[1]DOY		(kg ha^{-1})	(kg ha^{-1})	(kg ha^{-1})	(kg ha^{-1})	(kg ha^{-1})	(kg ha^{-1})	
198	E	0.55 ± 0.18a	0.54 ± 0.17a	0.54 ± 0.17a	0.55 ± 0.16a	0.56 ± 0.18a	0.52 ± 0.19a	0.54 ± 0.18
209	V4	0.50 ± 0.21a	0.50 ± 0.20a	0.50 ± 0.20a	0.50 ± 0.22a	0.49 ± 0.26a	0.46 ± 0.27a	0.49 ± 0.23
216	V6	0.56 ± 0.17b	0.50 ± 0.21ba	0.46 ± 0.26ba	0.41 ± 0.30ba	0.33 ± 0.38ba	0.32 ± 0.38a	0.43 ± 0.28
230	V10	0.37 ± 0.32b	0.27 ± 0.36ba	0.13 ± 0.40ba	0.09 ± 0.43ba	-0.05 ± 0.46a	-0.07 ± 0.43a	0.12 ± 0.40
244	PF	0.23 ± 0.38c	0.02 ± 0.43cb	-0.13 ± 0.47cba	-0.23 ± 0.50ba	-0.42 ± 0.48ba	-0.50 ± 0.44a	-0.17 ± 0.45
256	FF	0.45 ± 0.24d	0.37 ± 0.27dc	0.30 ± 0.31dc	0.21 ± 0.33cb	0.03 ± 0.35ba	0.01 ± 0.31a	0.23 ± 0.30
265	GF	0.42 ± 0.21c	0.43 ± 0.25c	0.39 ± 0.24cb	0.33 ± 0.26cba	0.22 ± 0.28ba	0.25 ± 0.24a	0.34 ± 0.25
279	PM	0.26 ± 0.38a	0.35 ± 0.39a	0.32 ± 0.39a	0.32 ± 0.40a	0.29 ± 0.40a	0.31 ± 0.39a	0.31 ± 0.39
Average	-	0.42 ± 0.26	0.37 ± 0.29	0.32 ± 0.31	0.27 ± 0.33	0.18 ± 0.34	0.16 ± 0.33	0.29 ± 0.31

[1]DOY – Day of the Year

[2]CS: Crop stages; E – Emergence; Vegetative stages: V4 – Plants with four leaves per plant; V6 – Plants with six leaves per plant, and V10 – Plants with ten leaves per plant; Reproductive stages: PF – Pre flowering, FF – Full flowering, GF - Grain filling, and PM- Physiological maturation.

The H/R_n values with the same letter in each line indicate no significant differences from each other at 5% (pairwise comparisons using the Tuckey HSD post-hoc test performed by group with six repetitions for each CS.

As for the R_n partition into λE, no significative differences arise on H/R_n values from E to V4 and PM, however, it is perceived large variations from PF to GF, evidenced by the Tuckey HSD post-hoc test, with averages ranging from above 0.50 in July 17 (E) to below -0.40 in September 01 (PF) for L4 and L5. The negative H/R_n values in PF for L4 to L5 means more often occasions of additional energy coming from dryer areas to corn parcels under good root-zone moisture levels after rainfall, increasing λE above R_n. The high SD values for H/R_n ranging from 43 to 64% of the mean pixel values indicated large variabilities in the heating (high H) and cooling conditions (low H) for corn plants [4-6, 8, 30].

Drops on P from September to October together with increasing R_G levels during the crop stages V10 to PM reduced the partition of R_n to H, which impacted BIO [42]. The H/R_n values for corn in the current study are much larger than those reported by [2] from Landsat measurements in irrigated lemon inside the Atlantic Forest biome, who found annual averages of 0.30, 0.16, and 0.01 under drip, micro sprinkler, and pivot irrigation systems, respectively. These last lower values can be explained by the frequent occurrence of heat advection from the hotter areas at the vicinity of irrigated plots, reducing H rates from plants under good root-zone moisture conditions [43].

3.2.4 Spatial and Temporal Variations in Soil Heat Flux (G)

Figure 6 presents the G spatial distributions together with its pixel averages and SD regarding the whole corn area (a) and for each N cover fertilization level – L (b), considering the analyzed corn crop stages.

From Figure 6a, regarding the whole corn area, G increased along the growing season, starting with averages between 0.1 MJ m^{-2} d^{-1} in July 17 (E) and 0.7 MJ m^{-2} d^{-1} in September 13 (FF), when from this last CS dropped to 0.3 MJ m^{-2} d^{-1} from September 22 (GF) to October 06 (PM). Considering the spatial variations, they were very high, with SD representing 74% of the average in V4 (July 17 – August 04) to 177% during FF. However, as shown in Figure 6b, as for R_n, variations in average G daily values are very low when considering each specific N cover fertilization levels along the growing season. The G/R_n values but ranged from 0.1 MJ m^{-2} d^{-1} for L0 in V4 to 0.8 MJ m^{-2} d^{-1}in FF for L1. Besides crop stages, these values are also influenced by weather conditions, mainly R_G.

Table 4 shows the G/R_n average and SD values from remote sensing measurements and weather data, together with the results of the pairwise comparison by group, using the Tuckey HSD post-hoc test performed for the N cover fertilization levels in each corn CS.

As for R_n/R_G, there were low significative variations on G/R_n values among N cover fertilization level for each specific CS, evidenced by the Tuckey HSD post-hoc test. Among the energy balance components, the R_n partitions into G were the lowest one at daily timescale. The mean values of this ratio ranged from a minimum of 0.02 from July 17 (E) to July 28 (V4) from L0 to L2, without significant differences compared with the other N cover fertilization levels during these crop stages, increasing to peak of 0.09 in September 13 (FF) with L1.

The mean value of 0.04 for G/R_n including all N cover fertilization levels and crop stages means that on average only 4% of R_n was partitioned into G. For the Brazilian Atlantic Forest biome, G/R_n ranging from 0.03 to 0.24 was reported, with the high end of this range much larger than our ones for rainfed corn crop within this biome, but their rates involved urban areas [38].

However, a low average G/R_n value of 0.03 was found for natural vegetation in Caatinga biome within Northeast Brazil, like our mean value [44].

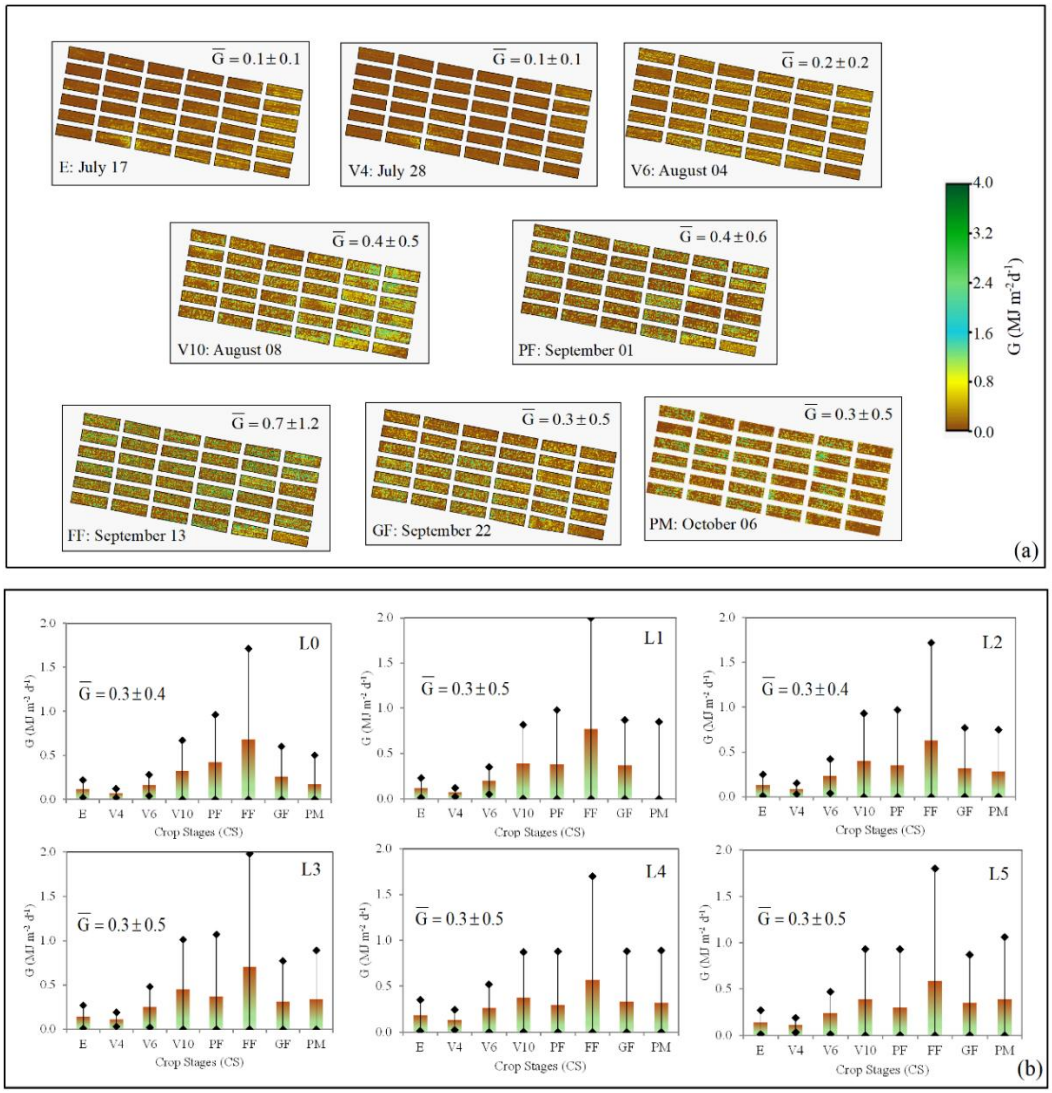

Figure 6 Spatial distribution of daily soil heat fluxes (G), together with its averages and standard deviations (SD), regarding the whole experimental area (a) and for each N cover fertilization – L[1] (b), involving the analyzed corn crop stages – CS[2], during the year 2022. [1]N Cover fertilization levels: L0 – N at 0 kg ha^{-1}; L1 – N at 25 kg ha^{-1}; L2 – N at 50 kg ha^{-1}; L3 – N at 100 kg ha^{-1}; L4 – N at 200 kg ha^{-1}; and L5 – N at 400 kg ha^{-1}. [2]Crop Stages: E – Emergency; V4, V6, and V10 – Vegetative stages with four, six, and ten leaves, respectively; Reproductive stages PF – Pre-flowering, FF – Full flowering, GF – Grain filling, and PM – Physiological maturation, respectively.

3.3 Remote sensing root-zone moisture indicators versus field measured crop parameters

Measured corn yield parameters offered the opportunity for assessing their relationships with remote sensing root-zone moisture indicators derived from the energy and water balance components. Figure 7 shows the relationships between BIO, Pr and harvest index (HI = Pr/BIO) with E_f (a) and r_s (b) for the corn growing season timescale.

It is clear, from the high determination coefficients (R^2 between 0.85 and 0.97), the strong influence of both E_f and r_s on BIO and Pr, being the best correlation for E_f and Pr (Figure 7a). However, the relations of HI with both root-zone moisture indicators were lower, R^2 of 0.55 for E_f (Figure 7a) and 0.51 for r_s (Figure 7b), respectively. These results show that root-zone moisture conditions have a strong effect on corn plants growth and vigor [11] and that one can accurately estimate BIO and Pr by modelling E_f and r_s with aerial cameras onboard UAV modelling energy and water balance components.

Table 4 Average pixel values and standard deviations (SD) for the ratio of soil heat flux (G) to net radiation (R_n) together with the Tuckey HSD post-hoc test performed by group, considering the N cover fertilizing levels for each corn crop stage (CS).

		Ratio of soil heat flux (G) to net radiation (R_n)						
N levels	CS[2]	L0: 0 (kg ha^{-1})	L1: 25 (kg ha^{-1})	L2: 50 (kg ha^{-1})	L3: 100 (kg ha^{-1})	L4: 200 (kg ha^{-1})	L5: 400 (kg ha^{-1})	Average
[1]DOY								
198	E	0.02 ± 0.01a	0.02 ± 0.01a	0.02 ± 0.02a	0.02 ± 0.02a	0.03 ± 0.01a	0.02 ± 0.02a	0.02 ± 0.01
209	V4	0.02 ± 0.01a	0.02 ± 0.01a	0.02 ± 0.01a	0.03 ± 0.02ab	0.03 ± 0.03b	0.03 ± 0.03b	0.02 ± 0.02
216	V6	0.03 ± 0.02a	0.04 ± 0.02ab	0.04 ± 0.03ab	0.04 ± 0.03ab	0.04 ± 0.04ab	0.04 ± 0.04b	0.04 ± 0.03
230	V10	0.04 ± 0.04a	0.05 ± 0.04a	0.05 ± 0.05a	0.06 ± 0.06a	0.05 ± 0.05a	0.05 ± 0.06a	0.05 ± 0.05
244	PF	0.06 ± 0.06a	0.05 ± 0.07a	0.05 ± 0.07a	0.05 ± 0.08a	0.04 ± 0.07a	0.04 ± 0.07a	0.05 ± 0.07
256	FF	0.08 ± 0.09a	0.09 ± 0.11a	0.07 ± 0.10a	0.08 ± 0.12a	0.07 ± 0.10a	0.07 ± 0.11a	0.07 ± 0.11
265	GF	0.03 ± 0.03a	0.04 ± 0.04a	0.03 ± 0.04a	0.03 ± 0.04a	0.03 ± 0.05a	0.04 ± 0.04a	0.03 ± 0.04
279	PM	0.02 ± 0.03a	0.04 ± 0.05ab	0.03 ± 0.04ab	0.04 ± 0.05ab	0.04 ± 0.05ab	0.04 ± 0.06b	0.04 ± 0.05
Average	-	0.04 ± 0.04	0.04 ± 0.04	0.04 ± 0.05	0.04 ± 0.05	0.04 ± 0.05	0.04 ± 0.05	0.04 ± 0.05

[1]DOY – Day of the Year

[2]CS: Crop stages; E – Emergence; Vegetative stages: V4 – Plants with four leaves per plant; V6 – Plants with six leaves per plant, and V10 – Plants with ten leaves per plant; Reproductive stages: PF – Pre flowering, FF – Full flowering, GF - Grain filling, and PM- Physiological maturation.

The G/R_n values with the same letter in each line indicate no significant differences from each other at 5% (pairwise comparisons using the Tuckey HSD post-hoc test performed by group with six repetitions for each CS.

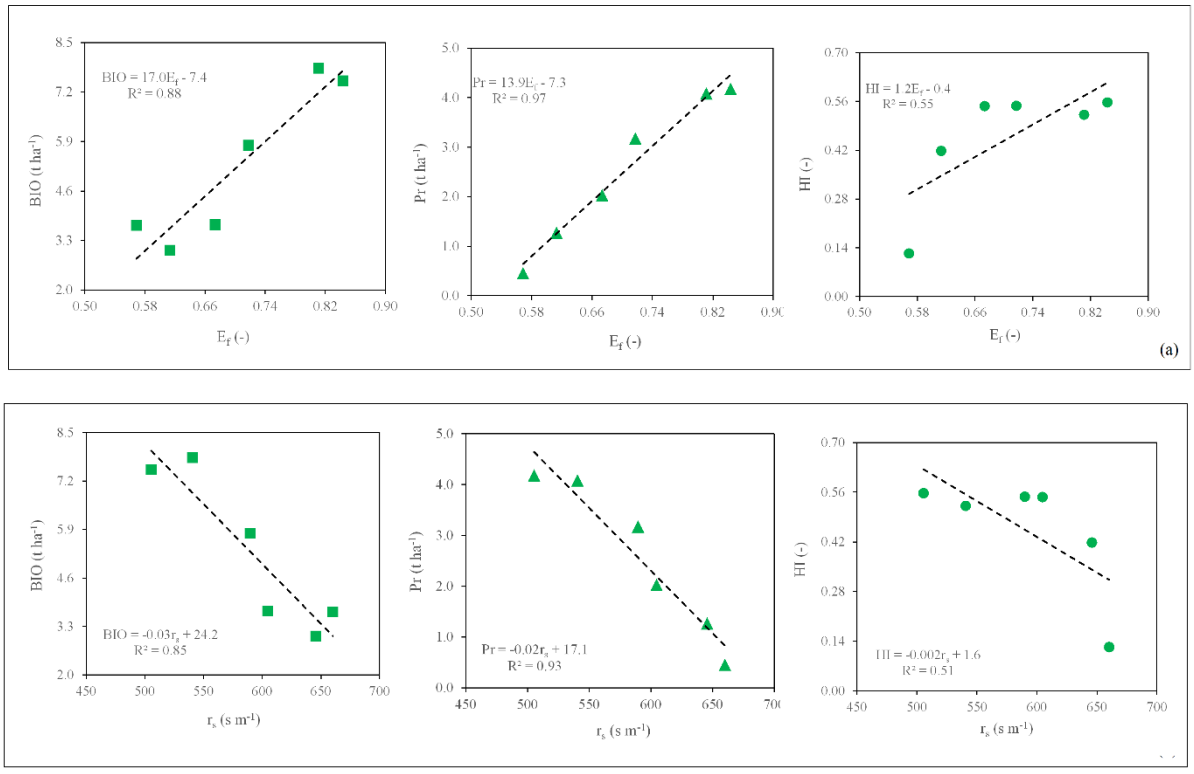

Figure 7 Relations between measured crop yield parameters and remote-sensing root-zone moisture indicators: (a) biomass production (BIO), productivity (Pr) and harvest index (HI) with evaporative fraction (E_f); and (b) BIO, Pr and HI with surface resistance (r_s).

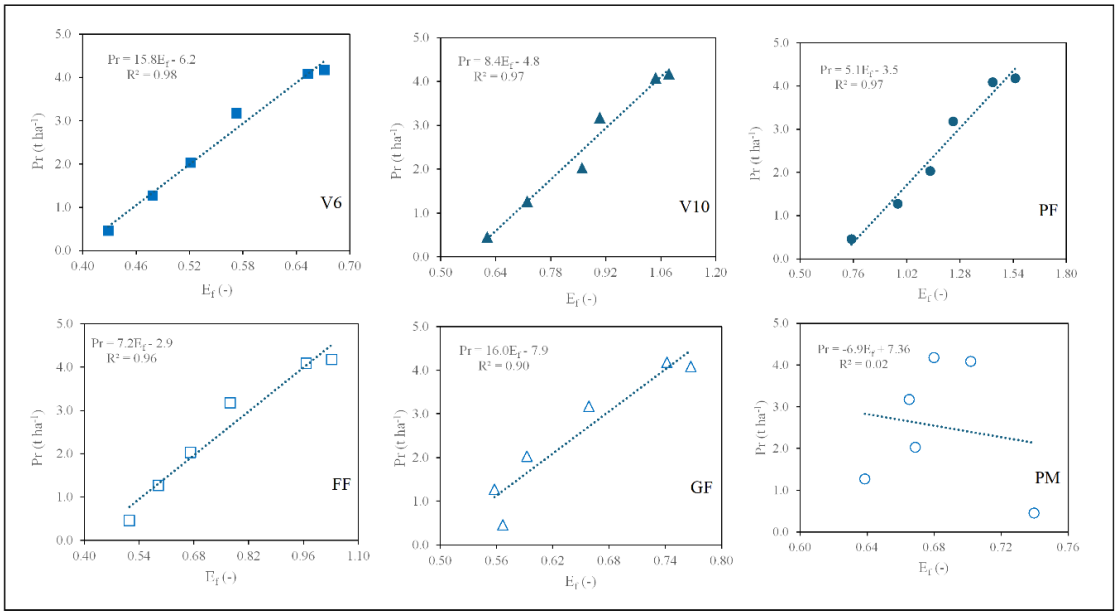

Figure 8 Relations between measured productivity (Pr) and the modelled evapotranspiration fraction (E_f) from corn crop stages V6 (plants with six leaves) to PM (physiological maturation).

Investigations on irrigated corn yield responses in Texas (EUA), confirmed the possibility of monitoring plant water deficiencies using physiological and environmental parameters [45]. With field experiments in Nebraska (USA), corn response to deficit irrigation was quantified to determine which water variables were best correlated to yield [20]. The authors found good correlations between evapotranspiration and yield, concluding that deficit-irrigating corn is not a good strategy under the conditions of their study. From field experiments under different irrigation strategies with corn crop in India, [11] confirmed that the effect of water deficit during PF and GF stages affects BIO, impacting Pr, according cultivar tolerance to water scarcity. Also, good relations between crop field measurements and remote sensing energy and water balance parameters were obtained by using images acquired from a Sequoia (Sq) camera in rainfed corn crop under different N cover fertilization levels in the Caatinga Brazilian biome [1].

As the effects of root-zone moisture on BIO depend on crop stages [11, 41], Figure 8 was built to investigate the relations of growing season Pr and E_f during corn crop stages V6 (plants with six leaves) to the PM (physiological maturation), aiming to see the suitability of predicting Pr before harvest.

Correlations between Pr and E_f declined from V6 to PM, being very poor at this last CS. The highest determination coefficient in V6 (R^2 = 0.98) means that Pr can be suitably predicted from the energy and water balance remote measurements before PM, supporting farmers for rational decisions about post-harvest actions. The low R^2 value of 0.02 in PM evidenced that yield is already defined in the previous crop stages, bringing much attention for crop management during V6, agreeing with [33], where it was pointed out that the conditions in this CS already define the potential production for corn crops. Predicting Pr from remote sensing E_f before Hvt can guide corn producers to make decisions about crop management and markets.

According to [11], water stress before PM in India affected corn performance, what agrees with R^2 above 0.90 during this CS in the current study. The authors found that low root-zone moisture levels increased the flowering days, days to maturity, anthesis silk interval, and decreased BIO dropping Pr. Studies on how corn morpho-physiological and BIO responded to varying soil moisture content during the early vegetative stage of two different hybrids of corn crop in Mississippi State (EUA), also concluded that physiology, morphology, and plant responses are affected by distinct root-zone moisture levels during the early-season crop stages [46]. According to these last authors, BIO dynamically changed with water stress intensity, and functional relationships can be used to predict plant performance and to improve crop management.

4. Conclusion

Assessments on corn energy and water balance components were possible with measurements taken with an unmanned aerial vehicle (UAV) by using only three reflectance bands of a Mapir camera, which together with weather data, dry matter and crop field data, allowed to account for the effects of different N cover fertilization levels on crop yield parameters.

An increase in net radiation (R_n) occurred during the growing season but mainly following global solar radiation (R_G), with the fraction R_n/R_G without significative differences among the N cover fertilization levels. However, strong distinctions on latent (λE) and sensible heat (H) fluxes were perceived varying these levels along the crop stages, which affected biomass production (BIO) and productivity (Pr). Peaks for λE occurred in the pre-flowering (PF), while for H, the maximums

occurred during emergency crop stage (E) with the lowest and negative values in the PF crop stage, indicating heat advection from the drier areas at the vicinity of corn plants. However, both λE and H later stabilized after the N level of 200 kg ha^{-1} for any N cover fertilization level, indicated that cover fertilizations above this level do not increase yield and could cause more impact by N lixiviation to the ground water. Among the energy balance components, soil heat flux (G) was the lowest one at daily timescale representing, on average, only 4% of the R_n for the growing season.

Relations of remote sensing root-zone moisture indicators with BIO and Pr evidenced their best correlation with the evapotranspiration fraction (E_f), but there were also good correlations with the surface resistance (r_s). These good correlations show that root-zone moisture conditions have a strong effect on corn plants growth and vigor and that one can accurately estimate BIO and Pr by modelling E_f and r_s with aerial cameras onboard UAV. Comparing Pr with E_f, the highest correlation when plants were with six leaves (V6) indicated that corn yield can be predicted from remote sensing measurements before harvest, confirming that the conditions before physiological maturation (PM) already define the potential productivity for corn crops, guiding corn producers to make decisions about crop management and markets.

It could be concluded that UAV modelling is useful for corn energy and water balance assessments under different crop managements, including nitrogen (N) cover fertilization under different N levels with possibility of replication in other regions, crops and managements with calibrations and validations of the key coefficients for r_s by simultaneous field and remote sensing measurements using the Penman-Monteith equation.

Abreviations

ANOVA	Analysis of Variance
CS	Crop Stages
DN	Digital numbers
DOY	Day of the Year
E	Emmergence
Hvt	Farvest
V4	Plant with four leaves
V6	Plant with six leaves
V10	Plant with ten leaves
PF	Pre Flowering
FF	Full Flowering
GF	Grain filling
PM	Physiological Maturation
N	Nitrogen
NDVI	Normalized Difference Vegetation Index
S	Sowing
SD	Standard Deviation
SUREAL	Surface Resistance Algorithm
UAV	Unmanned Aerial Vehicle

Symbols

BIO	Biomass Production
d	Zero Plane Displacement Height
E_f	Evapotranspiration Fraction
ET_0	Reference evapotranspiration
G	Soil Heat Flux
H	Soil Heat Flux
HSD	Honestly Significant Difference
k	von Karman's constant
L	Nitrogen cover fertilization level
L0	Nitrogen fertilization cover at 0 kg ha^{-1}
L1	Nitrogen fertilization cover at 25 kg ha^{-1}
L2	Nitrogen fertilization cover at 50 kg ha^{-1}
L3	Nitrogen fertilization cover at 100 kg ha^{-1}
L4	Nitrogen fertilization cover at 200 kg ha^{-1}
L5	Nitrogen fertilization cover at 400 kg ha^{-1}
P	Precipitation
Pr	Productivity
R_n	Net Radiation
r_a	Aerodynamic Resistance
R_G	Global Solar Radiatio
r_s	Surface Resistance
T_a	Mean Air Temperature
T_0	Surface Temperature
u_2	Wind Speed at 2 m
z_{0h}	Roughness Length governing of Heat and Vapor Transfer
z_{0m}	Roughness Length governing Momentum Transfer
z_2	Height of Wind Speed and Humidity at 2 m
α_0	Surffface Albedo
ε_a	Atmospheric Emissivity
ε_0	Surface Emissivity
σ	Stefan-Boltzmann Constant
τ	Transmisivity
λE	Latent Heat Flux
ρ	Reflectance

Author Contributions

Antônio Teixeira: Responsible for running the models, conceptualizations, energy and water balance assessments and writing the manuscript, processing image data, designing of figures, result analyses, software resources, and supervision. Diego Loureiro: Oversaw running of scripts, processing and formatting field data, methodology, data curation, validation, and editing of the manuscript. Jlyel Cruz: Processing and formatting field data, methodology, data curation, validation, and editing of the manuscript. Richard Souza: Processing and formatting field data, methodology, data curation, validation, and editing of the manuscript. Maria Gonzaga: Methodology, data curation, validation, and editing of the manuscript. Janice Leivas: Helped with processing the images, weather data, and result analyses. Celina Takemura: Helped with processing the images, weather data, and result analyses. André Almeida: Helped with processing the images, weather data, and result analyses.

Competing Interests

No conflicts of interest exist.

References

1. Teixeira A, Pacheco E, Silva C, Dompieri M, Leivas J. SAFER applications for water productivity assessments with aerial camera onboard a remotely piloted aircraft (RPA). A rainfed corn study in Northeast Brazil. Remote Sensing Applications: Society and Environment. 2021;22:100514.
2. Teixeira A, Leivas J, Struiving T, Reis J, Simão F. Energy balance and irrigation performance assessments in lemon orchards by applying the SAFER algorithm to Landsat 8 images. Agricultural Water Management. 2021;247:106725.
3. de Castro Teixeira AH, Leivas JF, Takemura CM, Pacheco EP, Garçon EAM, de Sousa IF, et al. Modeling and Monitoring Water Productivity by Using Geotechnologies: In Some Brazilian Agroecosystems. In: Remote Sensing Handbook, Volume V. CRC Press; 2024. p. 383–421.
4. Bhattarai N, Wagle P, Gowda PH, Kakani VG. Utility of remote sensing-based surface energy balance models to track water stress in rain-fed switchgrass under dry and wet conditions. ISPRS Journal of Photogrammetry and Remote Sensing. 2017;133:128–141.
5. Teixeira AHdC, Leivas JF, Hernandez FBT, Franco RAM. Large-scale radiation and energy balances with Landsat 8 images and agrometeorological data in the Brazilian semiarid region. Journal of Applied Remote Sensing. 2017;11(1):016030–016030.
6. de Castro Teixeira AH, Leivas JF, Ronquim CC, Bayma-Silva G. The use of MODIS images to quantify the energy balance in different agroecosystems in Brazil. In: Multi-purposeful application of geospatial data. London, UK: IntechOpen; 2018. p. 105–121.
7. Longo-Minnolo G, Vanella D, Consoli S, Intrigliolo D, Ramírez-Cuesta J. Integrating forecast meteorological data into the ArcDualKc model for estimating spatially distributed evapotranspiration rates of a citrus orchard. Agricultural Water Management. 2020;231:105967.
8. Teixeira A, Leivas J, Takemura C, Garçon E, Sousa I, Azevedo A. Monitoring anomalies on large-scale energy and water balance components by coupling remote sensing parameters and gridded weather data. International Journal of Biometeorology. 2024;68(12):2597–2612.
9. Allen RG, Pereira LS, Raes D, Smith M. Crop evapotranspiration-Guidelines for computing crop water requirements-FAO Irrigation and drainage paper 56 [Internet]. Rome, Italy: FAO; 1998. Available from: https://www.fao.org/4/x0490e/x0490e00.htm.
10. de Paula Almeida F, Junior JA, Knapp FM, Fernandes Souza JM, de Castro Teixeira AH, Evangelista AWP, et al. Impacts of corn flowering on estimation of evapotranspiration using remote sensing in Brazilian Savanna. Australian Journal of Crop Science. 2025;19(4):378–387.
11. Sah RP, Chakraborty M, Prasad K, Pandit M, Tudu V, Chakravarty M, et al. Impact of water deficit stress in maize: Phenology and yield components. Scientific reports. 2020;10(1):2944.
12. Venancio LP, Mantovani EC, Amaral CHd, Neale CMU, Filgueiras R, Gonçalves IZ, et al. Evapotranspiration mapping of commercial corn fields in Brazil using SAFER algorithm. Scientia Agricola. 2020;78(4):e20190261.
13. Bakhsh A, Jaynes DB, Colvin TS, Kanwar RS. Spatio-temporal analysis of yield variability for a corn-soybean field in Iowa. Transactions of the ASAE. 2000;43(1):31–38.
14. Maes WH, Steppe K. Perspectives for remote sensing with unmanned aerial vehicles in precision agriculture. Trends in plant science. 2019;24(2):152–164.
15. Manfreda S, McCabe MF, Miller PE, Lucas R, Pajuelo Madrigal V, Mallinis G, et al. On the use of unmanned aerial systems for environmental monitoring. Remote Sensing. 2018;10(4):641.
16. Tunca E, Köksal ES, Çetin S, Ekiz NM, Balde H. Yield and leaf area index estimations for sunflower plants using unmanned aerial vehicle images. Environmental monitoring and assessment. 2018;190(11):682.
17. Colaço AF, Bramley RG. Do crop sensors promote improved nitrogen management in grain crops? Field Crops Research. 2018;218:126–140.
18. Sharma LK, Bali SK. A review of methods to improve nitrogen use efficiency in agriculture. Sustainability. 2017;10(1):51.
19. Gago J, Douthe C, Coopman RE, Gallego PP, Ribas-Carbo M, Flexas J, et al. UAVs challenge to assess water stress for sustainable agriculture. Agricultural Water Management. 2015;153:9–19.
20. Payero JO, Melvin SR, Irmak S, Tarkalson D. Yield response of corn to deficit irrigation in a semiarid climate. Agricultural Water Management. 2006;84(1-2):101–112.
21. Traore SB, Carlson RE, Pilcher CD, Rice ME. Bt and non-Bt maize growth and development as affected by temperature and drought stress. Agronomy journal. 2000;92(5):1027–1035.
22. Bayma G, Nogueira SF, Adami M, Sano EE, Nunez DC, Santos PM, et al. Estimating forage mass in Brazilian pasture-based livestock production systems through satellite and climate data integration. Computers and Electronics in Agriculture. 2025;237:110496.
23. Molden D, Bin D, Loeve R, Barker R, Tuong T. Agricultural water productivity and savings: policy lessons from two diverse sites in China. Water Policy. 2007;9(S1):29–44.
24. Adak T, Kumar G, Chakravarty N, Katiyar R, Deshmukh P, Joshi H. Biomass and biomass water use efficiency in oilseed crop (Brassica juncea L.) under semi-arid microenvironments. Biomass and Bioenergy. 2013;51:154–162.
25. Shi X, Elmore A, Li X, Gorence NJ, Jin H, Zhang X, et al. Using spatial information technologies to select sites for biomass power plants: A case study in Guangdong Province, China. Biomass and Bioenergy. 2008;32(1):35–43.

26. Chen Y, Guerschman J, Shendryk Y, Henry D, Harrison MT. Estimating pasture biomass using sentinel-2 imagery and machine learning. Remote Sensing. 2021;13(4):603.
27. Olivera-Guerra L, Merlin O, Er-Raki S, Khabba S, Escorihuela MJ. Estimating the water budget components of irrigated crops: Combining the FAO-56 dual crop coefficient with surface temperature and vegetation index data. Agricultural Water Management. 2018;208:120–131.
28. Teixeira AHdC. Determining regional actual evapotranspiration of irrigated crops and natural vegetation in the São Francisco river basin (Brazil) using remote sensing and Penman-Monteith equation. Remote Sensing. 2010;2(5):1287–1319.
29. de Castro Teixeira A, Bastiaanssen WG, Ahmad M-u-D, Moura Md, Bos M. Analysis of energy fluxes and vegetation-atmosphere parameters in irrigated and natural ecosystems of semi-arid Brazil. Journal of Hydrology. 2008;362(1-2):110–127.
30. Teixeira AHdC, Hernandez FB, Andrade RG, Leivas JF, Bolfe EL. Energy balance with Landsat images in irrigated central pivots with corn crop in the São Paulo State, Brazil. Proc SPIE. 2014;9239. DOI: 10.1117/12.2067090.
31. Ribeiro MC, Metzger JP, Martensen AC, Ponzoni FJ, Hirota MM. The Brazilian Atlantic Forest: How much is left, and how is the remaining forest distributed? Implications for conservation. Biological conservation. 2009;142(6):1141–1153.
32. Procopio S, Cruz M, de Almeida M, de Jesus Junior L, Nogueira Junior L, de Carvalho H. Sealba: Region of high agricultural potential in Northeast Brazil [Internet]. Infoteca-e; 2019. Available from: https://www.infoteca.cnptia.embrapa.br/infoteca/handle/doc/1115857?locale=es.
33. Fancelli A, Dourado Neto D. Ecophysiology and Phenology (in Portuguese). In: Corn Yield. Livroceres; 2000.
34. Smith GM, Milton EJ. The use of the empirical line method to calibrate remotely sensed data to reflectance. International Journal of remote sensing. 1999;20(13):2653–2662.
35. De Bruin H, Stricker J. Evaporation of grass under non-restricted soil moisture conditions. Hydrological sciences journal. 2000;45(3):391–406.
36. Peters AJ, Walter-Shea EA, Ji L, Vina A, Hayes M, Svoboda MD. Drought monitoring with NDVI-based standardized vegetation index. Photogrammetric engineering and remote sensing. 2002;68(1):71–75.
37. Silva CdOF, de Castro Teixeira AH, Manzione RL. Agriwater: An R package for spatial modelling of energy balance and actual evapotranspiration using satellite images and agrometeorological data. Environmental modelling & software. 2019;120:104497.
38. Funari FL, Pereira Filho AJ. Energy balance in a patch of the Atlantic Forest in São Paulo city, Brazil. Journal of Water Resource and Protection. 2014;6(9):805–812.
39. DeJonge K, Ascough Ii J, Andales A, Hansen N, Garcia L, Arabi M. Improving evapotranspiration simulations in the CERES-Maize model under limited irrigation. Agricultural Water Management. 2012;115:92–103.
40. Ding R, Kang S, Li F, Zhang Y, Tong L. Evapotranspiration measurement and estimation using modified Priestley–Taylor model in an irrigated maize field with mulching. Agricultural and Forest Meteorology. 2013;168:140–148.
41. Rosa R, Ramos T, Pereira L. The dual Kc approach to assess maize and sweet sorghum transpiration and soil evaporation under saline conditions: Application of the SIMDualKc model. Agricultural Water Management. 2016;177:77–94.
42. Sun Y, Fu R, Dickinson R, Joiner J, Frankenberg C, Gu L, et al. Drought onset mechanisms revealed by satellite solar-induced chlorophyll fluorescence: Insights from two contrasting extreme events. Journal of Geophysical Research: Biogeosciences. 2015;120(11):2427–2440.
43. Consoli S, Papa R. Corrected surface energy balance to measure and model the evapotranspiration of irrigated orange orchards in semi-arid Mediterranean conditions. Irrigation science. 2013;31(5):1159–1171.
44. da Silva PF, de Sousa Lima JR, Antonino ACD, Souza R, de Souza ES, Silva JRI, et al. Seasonal patterns of carbon dioxide, water and energy fluxes over the Caatinga and grassland in the semi-arid region of Brazil. Journal of Arid Environments. 2017;147:71–82.
45. Ko J, Piccinni G. Corn yield responses under crop evapotranspiration-based irrigation management. Agricultural Water Management. 2009;96(5):799–808.
46. Vennam RR, Ramamoorthy P, Poudel S, Reddy KR, Henry WB, Bheemanahalli R. Developing functional relationships between soil moisture content and corn early-season physiology, growth, and development. Plants. 2023;12(13):2471.